

Aziridinium lead iodide: a stable, low bandgap hybrid halide perovskite for photovoltaics

Chao Zheng* and Oleg Rubel*

Department of Materials Science and Engineering, McMaster University, 1280 Main Street West, Hamilton, Ontario L8S 4L8, Canada

E-mail: zhengc8@mcmaster.ca; rubelo@mcmaster.ca

Phone: +1647-936-1436; +1905-525-9140, ext. 24094

Abstract

The low ionization energy of an *A* site molecule is a very important factor, which determines the thermodynamical stability of $APbI_3$ hybrid halide perovskites, while the size of the molecule governs the stable phase at room temperature and, eventually, the bandgap. It is challenging to achieve both a low ionization energy and the reasonable size for the PbI_3 cage to circumvent the stability issue inherent to hybrid halide perovskites. Here we propose a new three-membered charged ring radical, which demonstrates a low ionization energy that renders a good stability for its corresponding perovskite and a reasonable cation size that translates into a suitable bandgap for the photovoltaic application. We use *ab initio* calculations to evaluate a polymorphism of the crystal structure of the proposed halide hybrid perovskite, its stability and electronic properties in comparison to the mainstream perovskites, such as the methylammonium and formamidinium lead iodide. Our results highlight the importance of van der Waals interactions for predicting a correct polymorphism of the perovskite *vs* hexagonal crystal structure.

Introduction

During the past ten years, halide hybrid perovskites increasingly catch researchers attentions as the absorber layers in photovoltaics.¹⁻⁵ Favorable electronic properties and a low-cost fabrication method give halide hybrid perovskites an advantage over the traditional silicon. One drawback of halide hybrid perovskites is their instability. The halide hybrid perovskites easily decompose under the influence of high temperature, oxygen, water, and even UV light.⁶⁻⁸ Zhang et al.⁹ pointed out that the instability of methylammonium (MA) lead iodide is intrinsic due to the similar total energies of the reactant and products obtained from the density-functional theory (DFT) calculation. To commercialize the hybrid halide perovskite photovoltaics, the stability issue should be resolved.

Many different ways are proposed to stabilize the perovskite structure. Some methods involved engineering of suitable device architectures, such as changing from a liquid electrolyte to a solid hole transport material. For the representative MA lead iodide $\text{CH}_3\text{NH}_3\text{PbI}_3$ based solar cells, the lifetime of hybrid halide perovskites increases from 10 minutes¹⁰ up to 1000 hours³ by substituting the iodide/iodine-based redox electrolyte with solid-state hole transport materials spiro-OMeTAD. Device encapsulation is also an effective strategy to prevent invasion of UV radiation, moisture or oxygen species.^{11,12} Although these methods indeed increase the stability of hybrid halide perovskite-based solar cells, the power conversion efficiencies still decrease by 60 % of the initial value after 1100 hours¹³ which is far from silicon solar panels that come on today's market with a 25-year long performance warranty. In this paper, we propose a new perovskite material with a highly unfavorable decomposition reaction enthalpy, which should stabilize it against degradation.

Hybrid halide perovskite structures discussed here are considered in the form of APbI_3 . Here A stands for an organic radical in the lead iodide framework. Based on our recent paper, the ionization energy of the molecule on A site (in addition to its size) can be an important factor which determines the stability of perovskites.¹⁴ A lower ionization energy of the cation favors a more stable structure. Organic molecules with the ionization energy lower than that

of MA are typically much larger in size than MA. For example, the guanidinium radical $C(NH_2)_3$ and tetramethylammonium radical $(CH_3)_4N$ show low ionization energies. The radii of these cations are 278 and 320 pm, respectively, vs 217 pm for MA that precludes formation of the perovskite structure in the lead iodide framework.¹⁴

Kieslich et al.¹⁵ proposed nitrogen-based cations, which were not used in perovskites before. From this group, an azetidinium radical $(CH_2)_3NH_2$ is promising due to its compact structure. This four-membered ring cation is larger than MA radical, but slightly smaller than the formamidinium radical $HC(NH_2)_2$. Recently, the azetidinium lead iodide $(CH_2)_3NH_2PbI_3$ was successfully synthesized.¹⁶ The crystal structure of quasicubic $(CH_2)_3NH_2PbI_3$ is shown in Fig. 1b. Pering et al.¹⁶ reported that $(CH_2)_3NH_2PbI_3$ demonstrates a very good stability when soaked in water in contrast to the MA lead iodide $CH_3NH_3PbI_3$. This observation correlates with the ionization energy of the $(CH_2)_3NH_2$ radical being 0.4 eV below that of MA.

Interestingly, there are also three-membered rings,¹⁷ of which the aziridinium radical $(CH_2)_2NH_2$ is a promising candidate to be used as the organic cation at *A* site of hybrid halide perovskites. Figure 1a illustrates a proposed quasicubic phase of $(CH_2)_2NH_2PbI_3$. This three-membered ring cation is only slightly larger than MA. As we will show below, the ionization energy of $(CH_2)_2NH_2$ is also much lower than that of MA. This fact implies that aziridinium lead iodide $(CH_2)_2NH_2PbI_3$ might be stable and suitable for photovoltaic applications. Here we discuss the structural stability and electronic properties of the new perovskite $(CH_2)_2NH_2PbI_3$. We also compare relevant electronic properties between $(CH_2)_2NH_2PbI_3$, $CH_3NH_3PbI_3$, and $(CH_2)_3NH_2PbI_3$.

Computational methods

An experimental structure of formamidinium iodide $HC(NH_2)_2I$ ¹⁸ was used as a parent structure for $(CH_2)_2NH_2I$ (Fig. 2) and $(CH_2)_3NH_2I$ salts. The hexagonal structures of

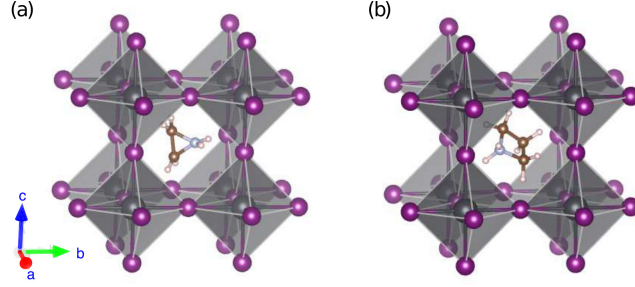


Figure 1: The quasicubic crystal structures of cyclic ring-based perovskites: (a) aziridinium lead iodide $(\text{CH}_2)_2\text{NH}_2\text{PbI}_3$ and (b) azetidinium lead iodide $(\text{CH}_2)_3\text{NH}_2\text{PbI}_3$.

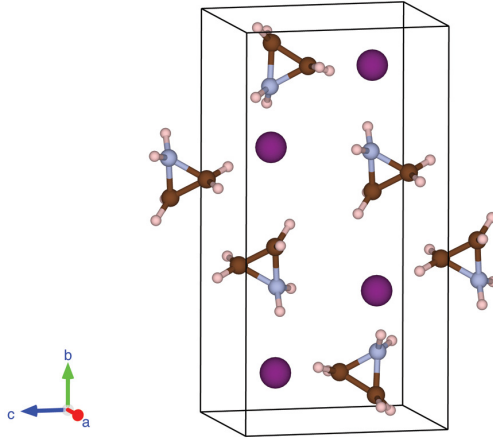


Figure 2: The crystal structure of aziridinium iodide $(\text{CH}_2)_2\text{NH}_2\text{I}$.

$\text{CH}_3\text{NH}_3\text{PbI}_3$, $(\text{CH}_2)_2\text{NH}_2\text{PbI}_3$ and $(\text{CH}_2)_3\text{NH}_2\text{PbI}_3$ are adapted from the hexagonal $\text{HC}(\text{NH}_2)_2\text{PbI}_3$.¹⁹ The crystal structures of $\text{CH}_3\text{NH}_3\text{PbBr}_3$ and $\text{CH}_3\text{NH}_3\text{PbCl}_3$ are obtained from Refs. 20 and 21, respectively. The crystal structures of MA halides are obtained from Refs. 22–24. Crystallographic information files (CIF) with atomic structures used in calculations can be accessed through the Cambridge crystallographic data centre (CCDC deposition numbers 1584308–1584327).

All calculations are based on DFT method.²⁵ Perdew-Burke-Ernzerhof (PBE) generalized gradient approximation²⁶ is used for the exchange-correlation functional. Dispersion interactions are included at the DFT-D3 level.²⁷ To predict the bandgaps of perovskites, a many body perturbation theory, within the *GW* approach,^{28,29} is utilized including the spin-orbit coupling (SOC). Vienna *ab initio* simulation program (VASP) and projector augmented-wave potentials are used to perform all the calculations.^{30–32} Monopole, dipole and quadrupole

corrections implemented in VASP^{33,34} were used to eliminate leading errors and acquiring accurate total energies of all charged ions.

For reciprocal space integration, $4 \times 4 \times 4$ Monkhorst-Pack grid³⁵ was used for cubic perovskite phases, $5 \times 5 \times 3$ for tetragonal perovskite phases, $4 \times 4 \times 4$ for hexagonal phases, $5 \times 5 \times 3$ for orthorhombic perovskite phases, and $6 \times 2 \times 4$ for the triclinic phases of $(\text{CH}_2)_2\text{NH}_2\text{I}$ and $(\text{CH}_2)_3\text{NH}_2\text{I}$. The convergence of reaction enthalpies with respect to the k-mesh density is achieved better than 5 meV, which was tested by doubling the density for several perovskite structures and their reactants. The cutoff energy for a plane wave expansion was set at 500 eV. The lattice constant and atomic positions were optimized such that residual forces acting on atoms did not exceed 2 meV/Å, and the residual hydrostatic pressure was less than 50 MPa.

Results and discussion

Stability of aziridinium lead iodide $(\text{CH}_2)_2\text{NH}_2\text{PbI}_3$

Formability of inorganic perovskite structures can be rationalized via geometrical factors such as the Goldschmidt’s tolerance factor³⁶ and Pauling’s octahedral factor.³⁷ To calculate the geometrical factors of hybrid halide perovskites, the effective organic cation radii should be estimated. Following Kieslich et al.¹⁵ the organic cation radius can be expressed as

$$r_{\text{eff}} = r_{\text{mass}} + r_{\text{ion}}, \tag{1}$$

where r_{mass} is the distance between the centre of mass of the molecule and the atom with the largest distance to the centre of mass (excluding hydrogen atoms) and r_{ion} is the corresponding ionic radius of this atom. The effective radii of three- and four-membered ring cations are listed in Table 1 along the side with the representative organic and inorganic cations. The size of cyclic cations is between that of MA and formamidinium.

Table 1: Geometrical factors of selected perovskites and calculated ionization energies of corresponding A site cations

Radical A	A^+ cation radius (pm)	Tolerance factor for $APbI_3$	Ionization energy (eV)	
			DFT ^a	Exp.
Cs	181	0.81	3.85	3.89 ⁴²
CH ₃ NH ₃	215	0.91	4.36	4.30±0.1 ⁴³
(CH ₂) ₂ NH ₂	227	0.93	4.07	...
(CH ₂) ₃ NH ₂	250	0.98	3.96	...
HC(NH ₂) ₂	264	1.01	4.18	...

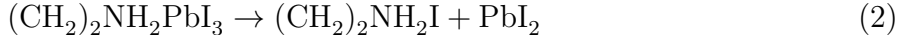
^a The ionization energies are obtained from the PBE total energy difference of cations and neutral radicals including the vibrational zero-point energy.

The cation effective radii are used to evaluate the Goldschmidt’s tolerance factor t for $APbI_3$ perovskite structures (Table 1). The tolerance factor of $(CH_2)_3NH_2PbI_3$ is too large to form a cubic or tetragonal structure ($t > 0.96$ ³⁸). Pering et al.¹⁶ reported the experimental band gap of $(CH_2)_3NH_2PbI_3$ which is about 2.15 eV. If the structure of $(CH_2)_3NH_2PbI_3$ was tetragonal or cubic, one would expect its band gap to be less than that of $CH_3NH_3PbI_3$ ($E_g < 1.6$ eV) due to a greater volume of the unit cell. The high experimental value of E_g can be attributed to a different crystal structure of $(CH_2)_3NH_2PbI_3$. For instance, theoretical calculations predict $E_g \approx 2.6$ eV for $CH_3NH_3PbI_3$ in a hexagonal phase.³⁹ Similarly, $HC(NH_2)_2PbI_3$ undergoes cubic to hexagonal phase transition at room temperature that is associated with an optical bleaching due to opening of the band gap.^{40,41}

According to our earlier study,¹⁴ the radical ionization energy at A site has an effect on the final reaction enthalpy of hybrid halide perovskites. The lower ionization energy, the more stable is the structure. The ionization energies of corresponding organic cations are presented in Table. 1. Both radicals $(CH_2)_2NH_2$ and $(CH_2)_3NH_2$ have the ionization energies lower than MA. Their values are close to the ionization energy of Cs which is the lowest one in the periodic table. This result suggests that $(CH_2)_2NH_2PbI_3$ and $(CH_2)_3NH_2PbI_3$ should be more stable than $CH_3NH_3PbI_3$.

To investigate the stability of $(CH_2)_2NH_2PbI_3$, we use the following decomposition reac-

tion equation



and the corresponding enthalpy

$$\Delta H_r = E_{\text{tot}}[(\text{CH}_2)_2\text{NH}_2\text{PbI}_3] - E_{\text{tot}}[(\text{CH}_2)_2\text{NH}_2\text{I}] - E_{\text{tot}}[\text{PbI}_2] . \quad (3)$$

The total energies E_{tot} of products and the reactant are evaluated using DFT. If the total energy of the products is lower than the total energy of the reactant, the perovskite structure is deemed unstable.⁹ This approach ignores finite temperature components of the free energy, which is of the order of -0.1 eV for $\text{CH}_3\text{NH}_3\text{PbI}_3$.⁴⁴

As a benchmark, we analyzed the stability and polymorphism of $\text{CH}_3\text{NH}_3\text{PbI}_3$. Among various polymorphs, we include a possibility for a hexagonal phase, since perovskite structures with large cations ($t > 0.96$) have a tendency to adapt a hexagonal phase. PBE is first used as the exchange-correlation functional. Results listed in Table 2 suggest that the hexagonal structure of $\text{CH}_3\text{NH}_3\text{PbI}_3$ has the lowest total energy at 0 K. This finding contradicts experimental data,⁴⁵⁻⁴⁷ according to which the tetragonal $\text{CH}_3\text{NH}_3\text{PbI}_3$ phase will undergo phase transformation to cubic structure above 327.4 K. The tetragonal $\text{CH}_3\text{NH}_3\text{PbI}_3$ phase will transform to the orthorhombic structure below 162.2 K. During the whole polymorphism transformation of $\text{CH}_3\text{NH}_3\text{PbI}_3$, there is no hexagonal structure present. Recently, a theory-based study reported similar controversial results on the hexagonal $\text{CH}_3\text{NH}_3\text{PbI}_3$ to have the lowest total energy and predicted it is the stable low-temperature phase.³⁹ However, we are inclined to think that the hexagonal phase of $\text{CH}_3\text{NH}_3\text{PbI}_3$ is probably a metastable phase. It is the choice of the exchange-correlation functional that is a possible reason for DFT failure to accurately predict the correct polymorphism transformation order of $\text{CH}_3\text{NH}_3\text{PbI}_3$. Thus, different exchange-correlation functionals are employed to evaluate the polymorphism transformation of $\text{CH}_3\text{NH}_3\text{PbI}_3$ (see in Fig. 3).

Figure 3 illustrates the total energies of different phases of $\text{CH}_3\text{NH}_3\text{PbI}_3$ obtained us-

Table 2: Polymorphism of hybrid halide perovskites predicted using DFT with and without the van der Waals correction.

Compound	Phase	PBE		PBE+vdW(D3)	
		E_{tot} (meV)	ΔH_r (meV)	E_{tot} (meV)	ΔH_r (meV)
$\text{CH}_3\text{NH}_3\text{PbI}_3$	Cubic	111	71	122	160
	Tetragonal	79	39	44	82
	Orthorhombic	58	18	0	38
	Hexagonal	0	-40	11	49
$(\text{CH}_2)_2\text{NH}_2\text{PbI}_3$	Cubic	107	-44	67	-81
	Tetragonal	141	-10	54	-93
	Orthorhombic	140	-12	63	-84
	Hexagonal	0	-151	0	-147
$(\text{CH}_2)_3\text{NH}_2\text{PbI}_3$	Cubic	174	-51	73	-199
	Tetragonal	194	-31	99	-173
	Orthorhombic	171	-54	71	-201
	Hexagonal	0	-225	0	-272
$\text{HC}(\text{NH}_2)_2\text{PbI}_3$	Cubic	296	179	238	266
	Tetragonal	142	25	50	79
	Orthorhombic	113	-4	32	61
	Hexagonal	0	-117	0	29
$\text{CH}_3\text{NH}_3\text{PbBr}_3$	Cubic	71	13
	Orthorhombic	0	-58
$\text{CH}_3\text{NH}_3\text{PbCl}_3$	Cubic	68	-41
	Orthorhombic	0	-109

ing PBE, PBE+ZPE (zero point energy correction), PBE+vdW(D3),²⁷ PBEsol^{48,49} and SCAN⁵⁰ exchange-correlation functionals. Interestingly, all methods except for the the PBE+vdW(D3) favor the hexagonal structure at low temperature. The result indicates the importance of dispersion interactions to stabilize the low-temperature orthorhombic $\text{CH}_3\text{NH}_3\text{PbI}_3$. Li and Rinke⁵¹ pointed out that the van der Waals (vdW) correction is also essential to obtain an accurate lattice constant of hybrid halide perovskites. It should be noted that Thind et al.³⁹ performed similar calculations including vdW-correction, and their results showed that the hexagonal phase still has the lowest total energy among all the phases, which contradicts our results. We suspect that the reason for discrepancy can be a suboptimal structure of the orthorhombic phase used by Thind et al.³⁹.

Since van der Waals effects are important for the polymorphism of $\text{CH}_3\text{NH}_3\text{PbI}_3$, the

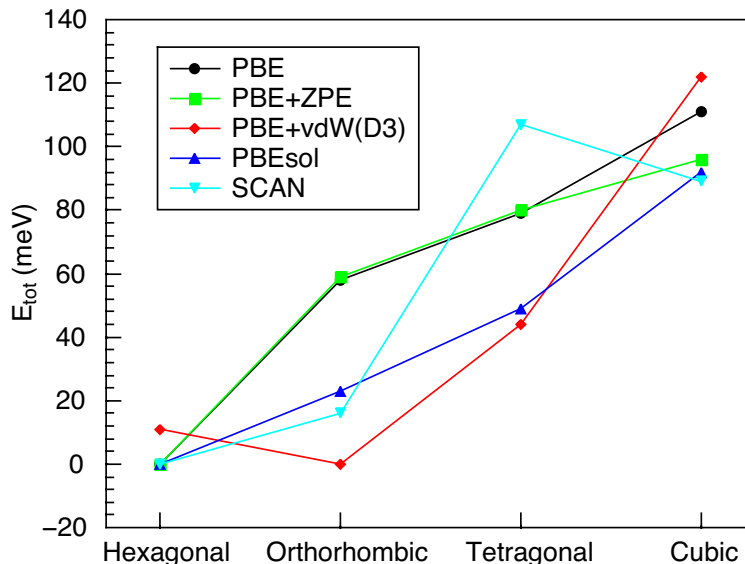


Figure 3: Polymorphism of $\text{CH}_3\text{NH}_3\text{PbI}_3$ with different exchange-correlation functionals. The origin of the energy scale is set at the lowest energy structure for each computational technique used.

same can be extended for other types of hybrid halide perovskites. Thus we focus on results obtained with PBE+vdW(D3) exchange-correlation functional in the remaining part of the paper. Table 2 lists the results of polymorphism prediction and corresponding decomposition reaction enthalpies for the perovskites of interest here. It is noticed that except $\text{CH}_3\text{NH}_3\text{PbI}_3$, all the other perovskites favor the hexagonal structures as the low-temperature stable phase. This trend can be attributed to a greater size of organic cations involved. For $\text{CH}_3\text{NH}_3\text{PbI}_3$ and $\text{HC}(\text{NH}_2)_2\text{PbI}_3$ ΔH_r values are weakly positive, which contradicts formability of those compounds. The final temperature contribution will lower the free energy down by approximately 0.1 eV^{44} making their formability feasible.

The Born-Haber cycles of APbI_3 hybrid halide perovskites indicate that the lower ionization energies of organic cations A will decrease the decomposition reaction enthalpies and further stabilize the corresponding perovskites.¹⁴ As evident from Table 1, the ionization energies of $(\text{CH}_2)_2\text{NH}_2$ and $(\text{CH}_2)_3\text{NH}_2$ are lower than those of $\text{HC}(\text{NH}_2)_2$ and MA. Accordingly, both reaction enthalpies of $(\text{CH}_2)_2\text{NH}_2\text{PbI}_3$ and $(\text{CH}_2)_3\text{NH}_2\text{PbI}_3$ in Table 2 are lower than those of $\text{CH}_3\text{NH}_3\text{PbI}_3$ and $\text{HC}(\text{NH}_2)_2\text{PbI}_3$. Thus, the three- and four-membered ring based

perovskites are more stable than the currently prevalent $\text{CH}_3\text{NH}_3\text{PbI}_3$ and $\text{HC}(\text{NH}_2)_2\text{PbI}_3$.

Recent comparative studies of stability among $\text{CH}_3\text{NH}_3\text{PbX}_3$ perovskites with $X = \text{Cl}$, Br , and I reported that a higher stability can be achieved by switching halide from I , to Br and Cl .^{8,9,52–55} Our calculated stability trend of $\text{CH}_3\text{NH}_3\text{PbX}_3$ is consistent with those observations. The lower reaction enthalpies of $(\text{CH}_2)_2\text{NH}_2\text{PbI}_3$ suggest that the stability of $(\text{CH}_2)_2\text{NH}_2\text{PbI}_3$ will be superior to $\text{CH}_3\text{NH}_3\text{PbCl}_3$ (Table 2).

Moreover, Tenuta et al.⁴⁴ indicated that the degradation of APbI_3 perovskites in the moist environment is governed by the solubility of a AI salt. The saturation concentration c_s of AI in the solvent exponentially depends on the reaction enthalpy given by Eq. (3). Considering a low reaction enthalpy of $(\text{CH}_2)_3\text{NH}_2\text{PbI}_3$, its decomposition via solvation of $(\text{CH}_2)_3\text{NH}_2\text{I}$ in water will be hindered. This prediction is consistent with the very low solubility of $(\text{CH}_2)_3\text{NH}_2\text{I}$ and the exceptional moisture stability of $(\text{CH}_2)_3\text{NH}_2\text{PbI}_3$.¹⁶

As we will see below, the band gap of $(\text{CH}_2)_2\text{NH}_2\text{PbI}_3$ is sensitive to its structure. For the photovoltaic application of this material, it is crucial that its structure adapts a cubic phase at the room temperature. As we discussed at the beginning of this section, the geometrical factors play an important role in formability of perovskites. Nagabhushana et al.⁵² showed the Goldschmidt’s tolerance factors of $\text{CH}_3\text{NH}_3\text{PbI}_3$ and $\text{CH}_3\text{NH}_3\text{PbBr}_3$ are 0.91 and 0.93, respectively. The $\text{CH}_3\text{NH}_3\text{PbBr}_3$ prefers cubic structure at the room temperature.^{45,46} It is suggested that MA is a relatively small cation for the PbI_3 framework, which results in a tetragonal phase at room temperature rather than the cubic one. Also, it seems that the $\text{HC}(\text{NH}_2)_2$ cation is too big for the PbI_3 framework to stay as a cubic phase around room temperature. The combination of MA cation and PbBr_3 framework is optimal to form a cubic phase with the tolerance factor of 0.93. Table 1 lists the tolerance factor of 0.93 for $(\text{CH}_2)_2\text{NH}_2\text{PbI}_3$. Thus, one can expect that both perovskites will exhibit a similar polymorphism as a function of temperature.

Besides, we found that the high-temperature phase transition point *vs* the energy difference between the low-temperature and high-temperature phases follows a linear trend

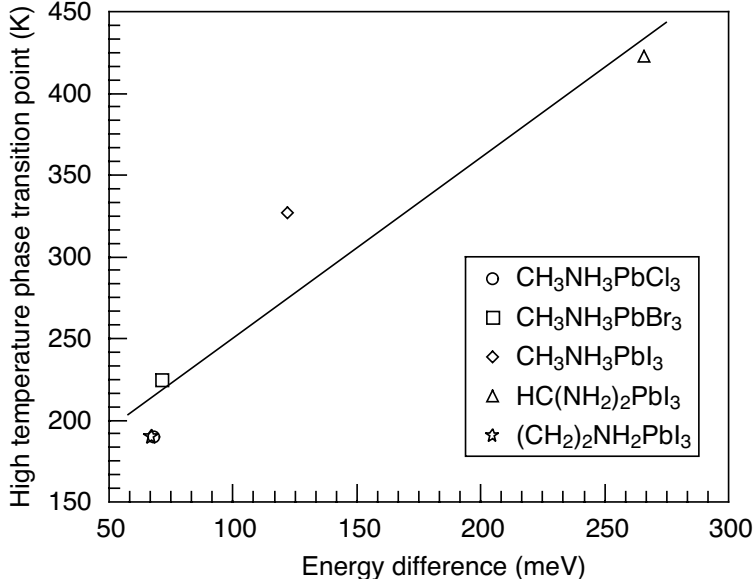


Figure 4: Correlation between the high-temperature phase transition point and the energy difference between the low-temperature phase and high-temperature phase. The linear line is a guide to the eye. High-temperature transition temperatures are taken from Refs. 45,46,56.

(see Fig. 4). From Fig. 4, energy difference between cubic and hexagonal structures of $(\text{CH}_2)_2\text{NH}_2\text{PbI}_3$ is 67 meV, which is close to the energy difference of 68 meV between cubic and orthorhombic structures of $\text{CH}_3\text{NH}_3\text{PbCl}_3$. The tetragonal $\text{CH}_3\text{NH}_3\text{PbCl}_3$ transitions to a cubic phase at 190 K. We expect $(\text{CH}_2)_2\text{NH}_2\text{PbI}_3$ to have the similar transition behavior and to adapt the cubic phase above 190 K.

Electronic properties of $(\text{CH}_2)_2\text{NH}_2\text{PbI}_3$

Till now, we found that the $(\text{CH}_2)_2\text{NH}_2$ radical has a very low ionization energy and a similar Goldschmidt's tolerance factor as $\text{CH}_3\text{NH}_3\text{PbBr}_3$. Based that, the $(\text{CH}_2)_2\text{NH}_2\text{PbI}_3$ perovskite solar cells should be more stable than $\text{CH}_3\text{NH}_3\text{PbI}_3$ and $\text{HC}(\text{NH}_2)_2\text{PbI}_3$. The key question remained unanswered is whether the proposed perovskite structure can serve as a solar cell absorber material? Here we report the band gap for the hypothetical $(\text{CH}_2)_2\text{NH}_2\text{PbI}_3$ obtained on the framework of *GW* approximation taking into account relativistic effects. It is known that bandgap is sensitive to the structural properties. The choice of a suitable exchange-correlation functional is determined by its ability to accurately predict the

Table 3: Lattice constants prediction of orthorhombic $\text{CH}_3\text{NH}_3\text{PbI}_3$ with different exchange-correlation functionals

Functionals	Lattice constants (\AA)			Error(%)			Volume (\AA^3)	Error(%)
	a	b	c	a	b	c		
Exp. ⁴⁷	8.81	12.59	8.56	–	–	–	949	–
PBE	9.23	12.86	8.63	4.8	2.2	0.8	1025	7.9
PBE+vdW(D3)	8.92	12.72	8.51	1.2	1.1	-0.5	966	1.7
PBEsol	8.96	12.61	8.43	1.7	0.2	-1.5	953	0.4
SCAN	8.93	12.69	8.53	-0.4	-0.3	-0.4	974	2.6

lattice parameters. Since bare DFT calculations are limited to 0 K, we compare the lattice parameters calculated with different exchange-correlation functionals considering the low-temperature orthorhombic phase of $\text{CH}_3\text{NH}_3\text{PbI}_3$. Results for PBE, PBE+vdW(D3), PBEsol and SCAN functionals are listed in Table 3.

We found that the PBE+vdW(D3), PBEsol, and SCAN exchange-correlation functionals can provide a reasonable prediction for the lattice constants. Here, we continue to use PBE+vdW(D3) optimized perovskite structures in order to remain consistent with the section on stability calculations. Results for bandgaps obtained using PBE+vdW(D3) exchange-correlation functional with and without SOC effect are shown in Table 4.

It is well known that DFT calculations with SOC grossly underestimates the bandgap of perovskites.⁵⁷ In Table 4, the calculated bandgaps with PBE+vdW(D3)+SOC are approximately 1 eV lower than the result without SOC. Bandgaps increase from cubic phase to hexagonal phase. Polymorphs of $(\text{CH}_2)_3\text{NH}_2\text{PbI}_3$ demonstrate the largest bandgaps among the four perovskites studied here. Bandgaps of different phases of $(\text{CH}_2)_2\text{NH}_2\text{PbI}_3$ lies between $\text{CH}_3\text{NH}_3\text{PbI}_3$ and $\text{HC}(\text{NH}_2)_2\text{PbI}_3$. It is obvious that hexagonal phases show much large bandgaps than perovskite phases. Thus, the hexagonal phase around room temperature is not desirable when aiming at photovoltaic applications.

Figure 5 shows a relativistic band structure of quasicubic $(\text{CH}_2)_2\text{NH}_2\text{PbI}_3$. The fundamental band gap is near R-point of the Brillouin zone. The presence of a Rashba splitting is noticeable at the vicinity of the band extrema, however its magnitude is heavily reduced

Table 4: Bandgaps (eV) of hybrid halide perovskites prediction with PBE+vdW(D3) and PBE+vdW(D3)+SOC

Compound	Phase	PBE+vdW(D3)	PBE+vdW(D3)+SOC
$\text{CH}_3\text{NH}_3\text{PbI}_3$	Cubic	1.44	0.38
	Tetragonal	1.51	0.76
	Orthorhombic	1.72	0.86
	Hexagonal	2.53	2.20
$(\text{CH}_2)_2\text{NH}_2\text{PbI}_3$	Cubic	1.35	0.36
	Tetragonal	1.58	0.62
	Orthorhombic	1.53	0.58
	Hexagonal	2.74	2.35
$(\text{CH}_2)_3\text{NH}_2\text{PbI}_3$	Cubic	1.56	0.54
	Tetragonal	1.61	0.64
	Orthorhombic	1.71	0.67
	Hexagonal	2.69	2.31
$\text{HC}(\text{NH}_2)_2\text{PbI}_3$	Cubic	1.34	0.33
	Tetragonal	1.60	0.67
	Orthorhombic	1.66	0.67
	Hexagonal	2.52	2.20

when compared with the Rashba splitting at the $\text{CH}_3\text{NH}_3\text{PbI}_3$ band edges.⁵⁸⁻⁶¹ The Rashba splitting in halide hybrid perovskites originates from the strong spin-orbit interaction and distortions in the Pb-centred octahedron.^{60,61} A more centrosymmetric PbI_3 cage of the quasicubic structure and its larger volume can be a reason for the reduced Rashba splitting in $(\text{CH}_2)_2\text{NH}_2\text{PbI}_3$.

The Rashba splitting in hybrid halide perovskites introduces an effectively indirect bandgap, which prolongs the carrier lifetime.^{60,62} We expect the reduced Rashba splitting in $(\text{CH}_2)_2\text{NH}_2\text{PbI}_3$ not to impede its power conversion efficiency for photovoltaic applications, since a similar weaker splitting can be found in the band structures of $\text{HC}(\text{NH}_2)_2\text{PbI}_3$.⁶³ Recently, Yang et al.⁵ fabricated formamidinium-lead-halide-based perovskite solar cells with a certified 22.1% power conversion efficiency.

It is well known that a first-principle GW approximation with SOC can accurately predict the bandgaps of hybrid halide perovskites.^{57,59} First, we used a single-shot G_0W_0 approximation with SOC to evaluate the bandgaps of quasicubic phases for perovskites of interest

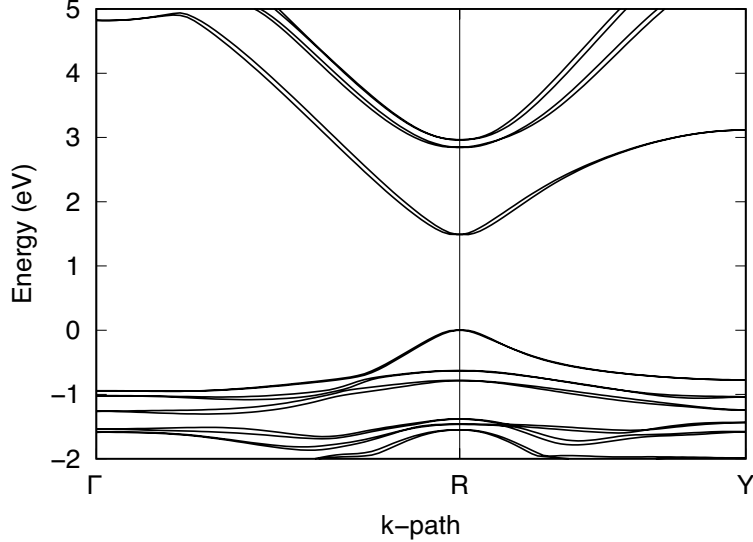


Figure 5: Electronic band structure of $(\text{CH}_2)_2\text{NH}_2\text{PbI}_3$ calculated at the PBE+SOC level with the band gap adjusted to match the G_0W_0 +SOC result in Table 5. The k -path includes the following high-symmetry points: $\Gamma(0, 0, 0)$, $\text{R}(0.5, 0.5, 0.5)$, and $\text{Y}(0, 0.5, 0)$.

Table 5: Quasiparticle bandgaps (eV) of various perovskites in the quasicubic phase.

Perovskites	G_0W_0 +SOC	GW_0 +SOC	Exp.	Reported GW +SOC
$\text{CH}_3\text{NH}_3\text{PbI}_3$	1.66	1.76	1.69 ⁶⁴	1.27–1.67 ^{59,64–67}
$(\text{CH}_2)_2\text{NH}_2\text{PbI}_3$	1.49	1.53
$(\text{CH}_2)_3\text{NH}_2\text{PbI}_3$	1.84	1.99
$\text{HC}(\text{NH}_2)_2\text{PbI}_3$	1.40	1.44	1.43–1.48 ^{56,68–70}	1.46 ⁷¹

(Table 5). Next, we carried out a partially self-consistent calculation by performing 4 iterations of G only (referred to as GW_0). The single-shot G_0W_0 method gave the best match of bandgaps with the experimental values (Table 5). Based on this table, we found that the bandgap of quasicubic $(\text{CH}_2)_2\text{NH}_2\text{PbI}_3$ is 0.17 eV lower than quasicubic $\text{CH}_3\text{NH}_3\text{PbI}_3$ and 0.09 eV higher than quasicubic $\text{HC}(\text{NH}_2)_2\text{PbI}_3$. This result suggests that $(\text{CH}_2)_2\text{NH}_2\text{PbI}_3$ may offer a superior utilization of the Sun’s spectrum than $\text{CH}_3\text{NH}_3\text{PbI}_3$.

Conclusions

In this paper, we proposed a three-membered cyclic organic cation based halide hybrid perovskite $(\text{CH}_2)_2\text{NH}_2\text{PbI}_3$ which has a potential to be used as the absorber material for photo-

voltaics. The low ionization energy of organic radical $(\text{CH}_2)_2\text{NH}_2$ decreases the reaction enthalpy of forming the corresponding perovskite. It suggests that this lower reaction enthalpy renders a much better stability of $(\text{CH}_2)_2\text{NH}_2\text{PbI}_3$ than $\text{CH}_3\text{NH}_3\text{PbI}_3$ and $\text{HC}(\text{NH}_2)_2\text{PbI}_3$. The appropriate cation radius of $(\text{CH}_2)_2\text{NH}_2$ for the PbI_3 framework and a low energy difference between high-temperature and low-temperature phases make $(\text{CH}_2)_2\text{NH}_2\text{PbI}_3$ transfer to a cubic phase feasible below the room temperature. Besides, we found that DFT calculation with PBE+vdW(D3) as the exchange-correlation functional can predict the correct order of polymorphism of $\text{CH}_3\text{NH}_3\text{PbI}_3$. Relativistic band structure plot demonstrates the existence of a Rashba splitting in $(\text{CH}_2)_2\text{NH}_2\text{PbI}_3$, albeit less prominent than in $\text{CH}_3\text{NH}_3\text{PbI}_3$. The Rashba splitting will allow $(\text{CH}_2)_2\text{NH}_2\text{PbI}_3$ to form an indirect bandgap near R-point in the Brillouin zone and benefit from an enhanced charge carrier lifetime. *GW* calculations suggest that the cubic phase of $(\text{CH}_2)_2\text{NH}_2\text{PbI}_3$ has an even lower bandgap of 1.49 eV than $\text{CH}_3\text{NH}_3\text{PbI}_3$ thereby making the former perovskite a suitable absorber material for solar cells.

Acknowledgement

Funding was provided by the Natural Sciences and Engineering Research Council of Canada under the Discovery Grant Program RGPIN-2015-04518. The work was performed using a Compute Canada infrastructure.

References

- (1) Kojima, A.; Teshima, K.; Shirai, Y.; Miyasaka, T. *J. Am. Chem. Soc.* **2009**, *131*, 6050–6051.
- (2) Kim, H. S.; Lee, C. R.; Im, J. H.; Lee, K. B.; Moehl, T.; Marchioro, A.; Moon, S. J.; Humphry Baker, R.; Yum, J. H.; Moser, J. E.; et al., *Sci. Rep.* **2012**, *2*, 591.

- (3) Lee, M. M.; Teuscher, J.; Miyasaka, T.; Murakami, T. N.; Snaith, H. J. *Science* **2012**, *338*, 643–647.
- (4) Eperon, G. E.; Burlakov, V. M.; Docampo, P.; Goriely, A.; Snaith, H. J. *Adv. Funct. Mater.* **2014**, *24*, 151–157.
- (5) Yang, W. S.; Park, B.-W.; Jung, E. H.; Jeon, N. J.; Kim, Y. C.; Lee, D. U.; Shin, S. S.; Seo, J.; Kim, E. K.; Noh, J. H.; et al., *Science* **2017**, *356*, 1376–1379.
- (6) Christians, J. A.; Herrera, P. A. M.; Kamat, P. V. *J. Am. Chem. Soc.* **2015**, *137*, 1530–1538.
- (7) Wozny, S.; Yang, M.; Nardes, A. M.; Mercado, C. C.; Ferrere, S.; Reese, M. O.; Zhou, W.; Zhu, K. *Chem. Mater.* **2015**, *27*, 4814–4820.
- (8) Buin, A.; Comin, R.; Xu, J.; Ip, A. H.; Sargent, E. H. *Chem. Mater.* **2015**, *27*, 4405–4412.
- (9) Zhang, Y. Y.; Chen, S.; Xu, P.; Xiang, H.; Gong, X. G.; Walsh, A.; Wei, S. H. *arXiv preprint arXiv:1506.01301* **2015**,
- (10) Im, J. H.; Lee, C. R.; Lee, J. W.; Park, S. W.; Park, N. G. *Nanoscale* **2011**, *3*, 4088–4093.
- (11) Gevorgyan, S. A.; Madsen, M. V.; Dam, H. F.; Jørgensen, M.; Fell, C. J.; Anderson, K. F.; Duck, B. C.; Mescheloff, A.; Katz, E. A.; Elschner, A.; et al., *Sol. Energ. Mat. Sol. Cells* **2013**, *116*, 187–196.
- (12) Zhou, H.; Chen, Q.; Li, G.; Luo, S.; Song, T. B.; Duan, H. S.; Hong, Z.; You, J.; Liu, Y.; Yang, Y. *Science* **2014**, *345*, 542–546.
- (13) Chauhan, A.; Kumar, P. *J. Phys. D* **2017**, *50*, 325105–325116.
- (14) Zheng, C.; Rubel, O. *J. Phys. Chem. C* **2017**, *121*, 11977–11984.

- (15) Kieslich, G.; Sun, S.; Cheetham, A. K. *Chem. Sci.* **2014**, *5*, 4712–4715.
- (16) Pering, S. R.; Deng, W.; Troughton, J. R.; Kubiak, P. S.; Ghosh, D.; Niemann, R. G.; Brivio, F.; Jeffrey, F. E.; Walker, A. B.; Islam, M. S.; Watson, T. M.; Raithby, P. R.; Johnson, A. L.; Lewis, S. E.; Cameron, P. J. *J. Mater. Chem. A* **2017**, *5*, 20658–20665.
- (17) Solka, B.; Russell, M. *J. Phys. Chem.* **1974**, *78*, 1268–1273.
- (18) Petrov, A. A.; Goodilin, E. A.; Tarasov, A. B.; Lazarenko, V. A.; Dorovatovskii, P. V.; Khrustalev, V. N. *Acta Crystallogr. Sect. E* **2017**, *73*, 569–572.
- (19) Stoumpos, C. C.; Malliakas, C. D.; Kanatzidis, M. G. *Inorg. Chem.* **2013**, *52*, 9019–9038.
- (20) Swainson, I.; Hammond, R.; Soulliere, C.; Knop, O.; Massa, W. *J. Solid State Chem.* **2003**, *176*, 97–104.
- (21) Chi, L.; Swainson, I.; Cranswick, L.; Her, J. H.; Stephens, P.; Knop, O. *J. Solid State Chem.* **2005**, *178*, 1376–1385.
- (22) Ishida, H.; Maeda, H.; Hirano, A.; Fujimoto, T.; Kubozono, Y.; Kashino, S.; Emura, S. *Z. Naturforsch. A.* **1995**, *50*, 876–880.
- (23) Gabe, E. *Acta Cryst.* **1961**, *14*, 1296–1296.
- (24) Hughes, E. W.; Lipscomb, W. N. *J. Am. Chem. Soc.* **1946**, *68*, 1970–1975.
- (25) Kohn, W.; Sham, L. J. *Phys. Rev.* **1965**, *140*, A1133.
- (26) Perdew, J. P.; Burke, K.; Ernzerhof, M. *Phys. Rev. Lett.* **1996**, *77*, 3865–3868.
- (27) Grimme, S.; Antony, J.; Ehrlich, S.; Krieg, H. *J. Chem. Phys.* **2010**, *132*, 154104.
- (28) Hedin, L. *Phys. Rev.* **1965**, *139*, A796–A823.
- (29) Hybertsen, M. S.; Louie, S. G. *Phys. Rev. B* **1986**, *34*, 5390–5413.

- (30) Kresse, G.; Furthmüller, J. *Phys. Rev. B* **1996**, *54*, 11169.
- (31) Kresse, G.; Joubert, D. *Phys. Rev. B* **1999**, *59*, 1758.
- (32) Blöchl, P. *Phys. Rev. B* **1994**, *50*, 17953.
- (33) Makov, G.; Payne, M. C. *Phys. Rev. B* **1995**, *51*, 4014–4022.
- (34) Neugebauer, J.; Scheffler, M. *Phys. Rev. B* **1992**, *46*, 16067–16080.
- (35) Monkhorst, H. J.; Pack, J. D. *Phys. Rev. B* **1976**, *13*, 5188.
- (36) Goldschmidt, V. M. *Naturwissenschaften* **1926**, *14*, 477–485.
- (37) Pauling, L. *J. Am. Chem. Soc.* **1929**, *51*, 1010–1026.
- (38) Feng, L.; Jiang, L.; Zhu, M.; Liu, H.; Zhou, X.; Li, C. *J. Phys. Chem. Solids* **2008**, *69*, 967–974.
- (39) Thind, A. S.; Huang, X.; Sun, J.; Mishra, R. *Chem. Mater.* **2017**, *29*, 6003–6011.
- (40) Weller, M. T.; Weber, O. J.; Frost, J. M.; Walsh, A. *J. Phys. Chem. Lett.* **2015**, *6*, 3209–3212.
- (41) Stoumpos, C. C.; Malliakas, C. D.; Peters, J. A.; Liu, Z.; Sebastian, M.; Im, J.; Chasapis, T. C.; Wibowo, A. C.; Chung, D. Y.; Freeman, A. J.; et al., *Cryst. Growth Des.* **2013**, *13*, 2722–2727.
- (42) Moore, C. E. *Ionization potentials and ionization limits derived from the analyses of optical spectra*; United States. Government Printing Office.: Washington D.C., 1970.
- (43) Jeon, S. J.; Raksit, A. B.; Gellene, G. I.; Porter, R. F. *J. Am. Chem. Soc.* **1985**, *107*, 4129–4133.
- (44) Tenuta, E.; Zheng, C.; Rubel, O. *Sci. Rep.* **2016**, *6*, 37654.

- (45) Poglitsch, A.; Weber, D. *J. Chem. Phys.* **1987**, *87*, 6373–6378.
- (46) Onoda-Yamamuro, N.; Matsuo, T.; Suga, H. *J. Phys. Chem. Solids.* **1990**, *51*, 1383–1395.
- (47) Whitfield, P.; Herron, N.; Guise, W.; Page, K.; Cheng, Y.; Milas, I.; Crawford, M. *Sci. Rep.* **2016**, *6*, 35685.
- (48) Perdew, J. P.; Ruzsinszky, A.; Csonka, G. I.; Vydrov, O. A.; Scuseria, G. E.; Constantin, L. A.; Zhou, X.; Burke, K. *Phys. Rev. Lett.* **2008**, *100*, 136406.
- (49) Csonka, G. I.; Perdew, J. P.; Ruzsinszky, A.; Philippsen, P. H. T.; Lebègue, S.; Paier, J.; Vydrov, O. A.; Ángyán, J. G. *Phys. Rev. B* **2009**, *79*, 155107.
- (50) Sun, J.; Ruzsinszky, A.; Perdew, J. P. *Phys. Rev. Lett.* **2015**, *115*, 036402.
- (51) Li, J.; Rinke, P. *Phys. Rev. B* **2016**, *94*, 045201.
- (52) Nagabhushana, G.; Shivaramaiah, R.; Navrotsky, A. *P. Natl. Acad. Sci. USA.* **2016**, *113*, 7717–7721.
- (53) Jong, U. G.; Yu, C. J.; Ri, J. S.; Kim, N. H.; Ri, G. C. *Phys. Rev. B* **2016**, *94*, 125139.
- (54) Mali, S. S.; Shim, C. S.; Hong, C. K. *NPG Asia Mater.* **2015**, *7*, e208.
- (55) Maculan, G.; Sheikh, A. D.; Abdelhady, A. L.; Saidaminov, M. I.; Haque, M. A.; Murali, B.; Alarousu, E.; Mohammed, O. F.; Wu, T.; Bakr, O. M. *J. Phys. Chem. Lett.* **2015**, *6*, 3781–3786.
- (56) Koh, T. M.; Fu, K.; Fang, Y.; Chen, S.; Sum, T.; Mathews, N.; Mhaisalkar, S. G.; Boix, P. P.; Baikie, T. *J. Phys. Chem. C* **2013**, *118*, 16458–16462.
- (57) Umari, P.; Mosconi, E.; De Angelis, F. *Sci. Rep.* **2014**, *4*, 4467.

- (58) Even, J.; Pedesseau, L.; Jancu, J. M.; Katan, C. *J. Phys. Chem. Lett.* **2013**, *4*, 2999–3005.
- (59) Brivio, F.; Butler, K. T.; Walsh, A.; van Schilfgaarde, M. *Phys. Rev. B* **2014**, *89*, 155204.
- (60) Zheng, F.; Tan, L. Z.; Liu, S.; Rappe, A. M. *Nano Lett.* **2015**, *15*, 7794–7800.
- (61) Rubel, O.; Bokhanchuk, A. *arXiv preprint arXiv:1508.03612* **2015**,
- (62) Stier, A. V.; McCreary, K. M.; Jonker, B. T.; Kono, J.; Crooker, S. A. *Nat. Commun.* **2016**, *7*, 10643.
- (63) Chen, T.; Chen, W. L.; Foley, B. J.; Lee, J.; Ruff, J. P.; Ko, J. P.; Brown, C. M.; Harriger, L. W.; Zhang, D.; Park, C.; et al., *Proc. Natl. Acad. Sci. U.S.A.* **2017**, *114*, 7519–7524.
- (64) Quarti, C.; Mosconi, E.; Ball, J. M.; D’Innocenzo, V.; Tao, C.; Pathak, S.; Snaith, H. J.; Petrozza, A.; De Angelis, F. *Energy Environ. Sci.* **2016**, *9*, 155–163.
- (65) Ahmed, T.; Salim, T.; Lam, Y.; Chia, E. E.; Zhu, J. X.; et al., *EPL* **2015**, *108*, 67015.
- (66) Bokdam, M.; Sander, T.; Stroppa, A.; Picozzi, S.; Sarma, D.; Franchini, C.; Kresse, G. *Sci. Rep.* **2016**, *6*, 28618.
- (67) Gao, W.; Gao, X.; Abtey, T. A.; Sun, Y. Y.; Zhang, S.; Zhang, P. *Phys. Rev. B* **2016**, *93*, 085202.
- (68) Pang, S.; Hu, H.; Zhang, J.; Lv, S.; Yu, Y.; Wei, F.; Qin, T.; Xu, H.; Liu, Z.; Cui, G. *Chem. Mater.* **2014**, *26*, 1485–1491.
- (69) Eperon, G. E.; Stranks, S. D.; Menelaou, C.; Johnston, M. B.; Herz, L. M.; Snaith, H. J. *Energy Environ. Sci.* **2014**, *7*, 982–988.
- (70) Stoumpos, C. C.; Kanatzidis, M. G. *Acc. Chem. Res.* **2015**, *48*, 2791–2802.

- (71) Arora, N.; Orlandi, S.; Dar, M. I.; Aghazada, S.; Jacopin, G.; Cavazzini, M.; Mosconi, E.; Gratia, P.; De Angelis, F.; Pozzi, G.; et al., *ACS Energy Lett.* **2016**, *1*, 107–112.

Graphical TOC Entry

